Identifying a cooperative control mechanism between an applied field and the environment of open quantum systems

Fang Gao,[1] Roberto Rey-de-Castro,[2] Yaoxiong Wang,[1,3] Herschel Rabitz,[2] and Feng Shuang[1,3,*]

[1]*Institute of Intelligent Machines, Chinese Academy of Sciences, Hefei 230031, China*

[2]*Department of Chemistry, Princeton University, Princeton, New Jersey 08544, USA*

[3]*Department of Automation, University of Science and Technology of China, Hefei 230027, China*

(Received 16 February 2016; published 9 May 2016)

Many systems under control with an applied field also interact with the surrounding environment. Understanding the control mechanisms has remained a challenge, especially the role played by the interaction between the field and the environment. In order to address this need, here we expand the scope of the Hamiltonian-encoding and observable-decoding (HE-OD) technique. HE-OD was originally introduced as a theoretical and experimental tool for revealing the mechanism induced by control fields in closed quantum systems. The results of open-system HE-OD analysis presented here provide quantitative mechanistic insights into the roles played by a Markovian environment. Two model open quantum systems are considered for illustration. In these systems, transitions are induced by either an applied field linked to a dipole operator or Lindblad operators coupled to the system. For modest control yields, the HE-OD results clearly show distinct cooperation between the dynamics induced by the optimal field and the environment. Although the HE-OD methodology introduced here is considered in simulations, it has an analogous direct experimental formulation, which we suggest may be applied to open systems in the laboratory to reveal mechanistic insights.

DOI: 10.1103/PhysRevA.93.053407

I. INTRODUCTION

The control of quantum systems, particularly utilizing optimization techniques, is showing increasing success [1–11]. Understanding the underlying mechanisms that achieve optimal control is a subject of much interest [2,12–17]. The Hamiltonian-encoding and observable-decoding (HE-OD) methodology has provided a feasible means for systematic mechanism extraction in closed quantum systems [18–26]. In HE-OD, a quantum pathway is defined as a set of physically relevant transitions connecting an initial to a final state(s), and the associated pathway amplitudes each have a modulus and phase extracted from the Dyson expansion that quantifies the pathway's importance in the underlying dynamics [18,27]. The mechanism extracted through the HE-OD procedure is given as the set of pathway amplitudes of significant magnitude. During an HE-OD experiment or simulation, the system Hamiltonian is perturbated (encoded) in a specific manner such that the resultant nonlinear distortion of a recorded output signal of the system can be analyzed (decoded) to extract the pathway amplitudes. In addition to mechanism extraction [25], this technique has also been further developed into a tool to guide the controls for the experimental or simulated manipulation of the significant pathways taken by the dynamics through the system's coupled set of states [26].

In practice, many quantum systems interact with their environment during the time that the control field is on. To explore the control mechanism in such open quantum systems, the effects of dissipative and dephasing processes have to be considered [28–35]. As a specific example, in the context of population transfer in multilevel systems, Shuang and Rabitz observed that optimal control fields and decoherence processes can cooperate with each other in the case of achieving modest control yields utilizing a strongly interacting environment [36]. However, the detailed nature of this cooperation reflected in the contributions of various types of quantum pathways (i.e., induced either by the external field or by the decoherence terms due to the environment) was not determined. Here, we revisit these circumstances to reveal the distinct cooperative contributions of the applied field and decoherence processes through an extension of HE-OD that allows for the treatment of open quantum systems. First, the theoretical framework of HE-OD for open quantum systems is developed. Then two simple model open quantum systems are considered to illustrate the treatment of environmental effects in the expanded open HE-OD technique. The results from application of HE-OD quantitatively demonstrate the nature of the cooperation between the field and the environment, confirming the previous qualitative analysis [36].

The paper is organized as follows. Section II introduces the theoretical framework of HE-OD for open quantum systems. Although HE-OD could be adopted to a variety of system-environment models, the present treatment considers the Markovian limit with a Lindblad term added to the dynamical equations. Section III illustrates the concepts with two multilevel quantum systems interacting with the environment, and HE-OD is employed to extract amplitudes clearly characterized as quantum pathways induced by either (i) the dipole, (ii) mixed dipole-environment interactions, or (iii) the environment. A discussion of the results and concluding remarks are given in Sec. IV. The latter section also provides a sketch of how HE-OD may be applied directly in the laboratory to open quantum systems.

II. HE-OD METHODOLOGY FOR OPEN QUANTUM SYSTEMS

A. The Lindblad equation in Liouville space

The state of a closed quantum system can be represented by a wave function $|\psi(t)\rangle$ whose evolution is governed by the

*shuangfeng@ustc.edu.cn

Schrödinger equation:

$$i\frac{d}{dt}|\psi(t)\rangle = [H_0 - \mu E(t)]|\psi(t)\rangle. \quad (1)$$

Here H_0 is the unperturbed Hamiltonian, μ is the transition dipole operator, $E(t)$ is the control field, and $\hbar$ has been absorbed into H_0 and μ for convenience.

With the eigenstates of H_0 as the basis set $\{|n\rangle, n = 1,2,\ldots,d\}$, the wave function can be expanded as $|\psi(t)\rangle = \sum_n |n\rangle c_n(t)$. The corresponding density operator

$$\rho(t) = |\psi(t)\rangle\langle\psi(t)| = \sum_{nm} \rho_{nm}(t)|n\rangle\langle m| \quad (2)$$

with

$$\rho_{nm}(t) = c_n(t)c_m^*(t)$$

evolves as

$$i\frac{d\rho(t)}{dt} = [H_0 - \mu E(t), \rho(t)]. \quad (3)$$

In the absence of interactions with the environment the evolution of the system is unitary. On the other hand, when the environmental effects are not negligible the system will follow nonunitary evolution. Assuming a Markovian environment, the evolution can be described by the Lindblad master equation [37]

$$\frac{\partial\rho(t)}{\partial t} = -i[H_0 - \mu E(t), \rho(t)] + \eta\mathcal{F}\{\rho(t)\}, \quad (4)$$

where

$$\mathcal{F}\{\rho(t)\} = \sum_{j=1}^{d^2-1}\left(L_j\rho L_j^+ - \frac{1}{2}L_j^+L_j\rho - \frac{1}{2}\rho L_j^+L_j\right), \quad (5)$$

with $\{L_j\}$ and η being, respectively, Lindblad operators and the system-environmental coupling strength parameter.

The density operator ρ can conveniently be written with double-bracket notation in Liouville space [38],

$$|\rho(t)\rangle\rangle = \sum_{m,n}\rho_{mn}(t)|mn\rangle\rangle, \quad (6)$$

and then Eq. (4) can be further simplified as

$$i\frac{d\rho_{jk}(t)}{dt} = \sum_{m,n}\mathcal{H}_{jk,mn}(t)\rho_{mn}(t), \quad (7)$$

which is similar to Eq. (1) except that the dimension here is the square of the corresponding dimension in Hilbert space. The structure of $\mathcal{H}$ is specifically shown in the illustrations in Sec. III.

B. HE-OD procedures

The definition of quantum pathways for open quantum systems is analogous to that for closed systems [18–20,22], but with the addition of environmentally induced transitions along with those that have the dual character of being associated with the system (i.e., dipole) and the environment simultaneously. In Liouville space, the density operator $|\rho(t)\rangle\rangle$ at time t evolves from the density operator $|\rho(0)\rangle\rangle$ at time 0, through the generally nonunitary evolution operator $\mathcal{U}(t)$,

$$|\rho(t)\rangle\rangle = \mathcal{U}(t)|\rho(0)\rangle\rangle. \quad (8)$$

The time dependence of the evolution operator can be derived from Eq. (7),

$$i\frac{d\mathcal{U}(t)}{dt} = \mathcal{H}(t)\mathcal{U}(t), \quad (9)$$

which can be expressed through a Dyson expansion in Liouville space,

$$\mathcal{U}(t) = I + (-i)\int_0^t \mathcal{H}(t_1)dt_1 + (-i)^2\int_0^t \mathcal{H}(t_2)\int_0^{t_2}\mathcal{H}(t_1)dt_1dt_2 + \cdots. \quad (10)$$

The transition amplitude from the the initial state $|aa\rangle\rangle$ (i.e., state $|a\rangle$ in Hilbert space) to the final state $|bb\rangle\rangle$ (i.e., state $|b\rangle$ in Hilbert space) is given by $\langle\langle bb|\mathcal{U}(t)|aa\rangle\rangle$, which can be written as a summation of quantum pathway amplitudes,

$$\langle\langle bb|\mathcal{U}(t)|aa\rangle\rangle = \sum_{n,\{lplq,\ldots\}}\mathcal{U}_{bb,aa}^{n(l'_{n-1}l_{n-1},l'_{n-2}l_{n-2},\ldots,l'_1l_1)}(t), \quad (11)$$

with

$$\mathcal{U}_{bb,aa}^{n(l'_{n-1}l_{n-1},l'_{n-2}l_{n-2},\ldots,l'_1l_1)}(t) = (-i)^n\int_0^t\langle\langle bb|\mathcal{H}(t_n)|l'_{n-1}l_{n-1}\rangle\rangle \times\int_0^{t_n}\langle\langle l'_{n-1}l_{n-1}|\mathcal{H}(t_{n-1})|l'_{n-2}l_{n-2}\rangle\rangle \times\ldots\times\int_0^{t_2}\langle\langle l'_1l_1|\mathcal{H}(t_1)|aa\rangle\rangle dt_1\ldots dt_{n-1}dt_n.$$

Here the amplitude $\mathcal{U}_{bb,aa}^{n(l'_{n-1}l_{n-1},l'_{n-2}l_{n-2},\ldots,l'_1l_1)}(t)$ corresponds to the transition from state $|aa\rangle\rangle$ to state $|bb\rangle\rangle$ through the sequence of n intermediate steps $|aa\rangle\rangle \to |l'_1l_1\rangle\rangle \to \cdots \to |l'_{n-2}l_{n-2}\rangle\rangle \to |l'_{n-1}l_{n-1}\rangle\rangle \to |bb\rangle\rangle$, which constitutes an nth-order pathway linking state$|aa\rangle\rangle$ and state$|bb\rangle\rangle$.

Similarly to the operations of HE-OD in a closed Hilbert space, the HE-OD methodology in Liouville space also consists of encoding the Hamiltonian $\mathcal{H}(t) \to \mathcal{H}(t,s)$ in a special fashion as a function of a variable s such that each relevant pathway amplitude in Eq. (11) has a unique signature in the output $\langle\langle bb|\mathcal{U}(t)|aa\rangle\rangle \to \langle\langle bb|\mathcal{U}(t,s)|aa\rangle\rangle$ [18,23,25,26]. In our simulations, an encoding is performed with the aid of the elements in the matrix Γ

$$\Gamma = \begin{pmatrix}\gamma_{11,11} & \gamma_{11,12} & \cdots & \gamma_{11,dd}\\ \gamma_{12,11} & \gamma_{12,12} & \cdots & \gamma_{12,dd}\\ \vdots & \vdots & \vdots & \vdots\\ \gamma_{dd,11} & \gamma_{dd,12} & \cdots & \gamma_{dd,dd}\end{pmatrix}, \quad (12)$$

and the detailed use of Γ is evident below and in the figures. Importantly, there is flexibility in the choice of the elements of Γ (some of which may be 0) in keeping with the goal of uniquely identifying the desired pathway amplitudes in

Eq. (11) from the output $\langle\langle bb|\mathcal{U}(t,s)|aa\rangle\rangle$ as a function of s.

In simulations, the HE-OD procedure consists of a sequence of N calculations at $s = 1,2,\ldots,N$, each resulting in an encoded system output [i.e., here, an element of $\mathcal{U}(t,s)$, on the left-hand side of Eq. (15)]. During the encoding step, any desired element of the Hamiltonian matrix $(\mathcal{H})_{jk,mn}$ can be modulated with an encoding function of s conveniently taken to have the Fourier form $\exp(2\pi i\gamma_{jk,mn}s/N)$ such that

$$(\mathcal{H})_{jk,mn} \rightarrow (\mathcal{H})_{jk,mn}e^{2\pi i\gamma_{jk,mn}s/N}, \quad s = 1,2,\ldots,N. \tag{13}$$

Then Eq. (9) becomes

$$i\frac{d\mathcal{U}(t,s)}{dt} = \begin{pmatrix} \mathcal{H}_{11,11}e^{2\pi i\gamma_{11,11}s/N} & \cdots & \mathcal{H}_{11,dd}e^{2\pi i\gamma_{11,dd}s/N} \\ \vdots & \vdots & \vdots \\ \mathcal{H}_{dd,11}e^{2\pi i\gamma_{dd,11}s/N} & \cdots & \mathcal{H}_{dd,dd}e^{2\pi i\gamma_{dd,dd}s/N} \end{pmatrix}\mathcal{U}(t,s), \tag{14}$$

whose solution is given by

$$\langle\langle bb|\mathcal{U}(t,s)|aa\rangle\rangle = \sum_{n,\{lplq,\ldots\}} \mathcal{U}_{bb,aa}^{n(l'_{n-1}l_{n-1},l'_{n-2}l_{n-2},\ldots,l'_1l_1)}(t) \times \mathcal{M}_{bb,aa}^{n(l'_{n-1}l_{n-1},l'_{n-2}l_{n-2},\ldots,l'_1l_1)}(s) \tag{15}$$

with

$$\mathcal{M}_{bb,aa}^{n(l'_{n-1}l_{n-1},l'_{n-2}l_{n-2},\ldots,l'_1l_1)}(s) = \exp\left[2\pi i\gamma_{n(l'_{n-1}l_{n-1},l'_{n-2}l_{n-2},\ldots,l'_1l_1)}s/N\right], \tag{16}$$

$$\gamma_{n(l'_{n-1}l_{n-1},l'_{n-2}l_{n-2},\ldots,l'_1l_1)} = \gamma_{bb,l'_{n-1}l_{n-1}} + \gamma_{l'_{n-1}l_{n-1},l'_{n-2}l_{n-2}} + \cdots + \gamma_{l'_1l_1,aa}. \tag{17}$$

The frequencies $\{\gamma_{jk,mn}\}$ are chosen as special positive integers (or 0 in some cases) to make the set of relevant frequencies $\gamma_{n(l'_{n-1}l_{n-1},l'_{n-2}l_{n-2},\ldots,l'_1l_1)}$ unique for each investigated specific pathway. As a result, the decoding functions $\mathcal{M}_{bb,aa}^{n(l'_{n-1}l_{n-1},l'_{n-2}l_{n-2},\ldots,l'_1l_1)}$ are orthogonal and unique for the investigated pathways:

$$\frac{1}{N}\sum_{s=1}^{N}\mathcal{M}_{bb,aa}^{n(l'_{n-1}l_{n-1},l'_{n-2}l_{n-2},\ldots,l'_1l_1)}(s)^*\mathcal{M}_{bb,aa}^{n'(p'_{n-1}p_{n-1},p'_{n-2}p_{n-2},\ldots,p'_1p_1)}(s) = \delta_{n(l'_{n-1}l_{n-1},l'_{n-2}l_{n-2},\ldots,l'_1l_1),n'(p'_{n-1}p_{n-1},p'_{n-2}p_{n-2},\ldots,p'_1p_1)}. \tag{18}$$

Due to their orthogonality, the amplitudes $\mathcal{U}_{bb,aa}^{n(l'_{n-1}l_{n-1},l'_{n-2}l_{n-2},\ldots,l'_1l_1)}(t)$ in Eq. (15), and, as a result, those in Eq. (11), can be readily computed by the inverse fast Fourier transform of the modulated matrix elements $\mathcal{U}_{bb,aa}(t,s)$. The physical interpretation of the extracted amplitudes can be understood through knowledge of the relation between the frequencies $\gamma_{n(l'_{n-1}l_{n-1},l'_{n-2}l_{n-2},\ldots,l'_1l_1)}$ and the corresponding pathways driven by the structure of the Lindblad equation and the meaning of the terms in Eq. (11).

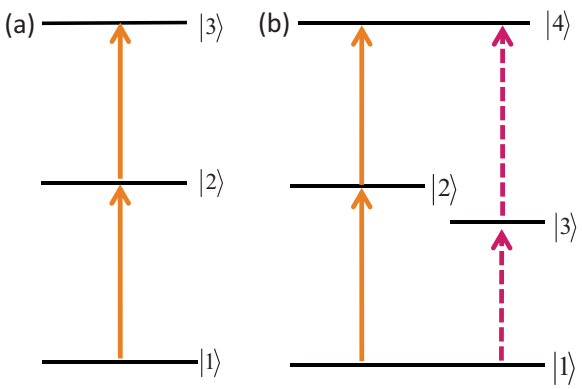

FIG. 1. Structure of the two quantum systems: model (a) and model (b). Arrows indicate dipole allowed transitions in each model.

III. ILLUSTRATIONS

In this section, the effect of the environment on the controlled quantum dynamics is explored in the context of population transfer from an initial state $|aa\rangle\rangle$ to a final state $|bb\rangle\rangle$. For convenience, the density operator in Liouville space is arranged as

$$|\rho(t)\rangle\rangle = \begin{pmatrix} \rho_{11} \\ \rho_{12} \\ \vdots \\ \rho_{1d} \\ \rho_{21} \\ \vdots \\ \rho_{dd} \end{pmatrix}. \tag{19}$$

Two different open quantum systems are employed to demonstrate the capabilities of the HE-OD procedure to extract the pathway amplitudes in Liouville space. As shown in Fig. 1, models (a) and (b) have, respectively, one and two routes linking the initial and target states. The figure shows that only the nearest-neighbor transitions are induced by dipole coupling in these systems. The Lindblad operators along with the numerical values of the parameters are chosen to induce the same transitions (i.e., only between nearest-neighbor levels) with comparable amplitudes as those by corresponding terms in the Hamiltonian. In this case, the environmental coupling is strong, consistent with the systems explored earlier [36]. The control fields $E(t)$ are taken to have the form

$$E(t) = e^{-\frac{(t-T/2)^2}{2\sigma^2}}\sum_l A_l\cos(\upsilon_l t + \theta_l), \tag{20}$$

where $T = 8268.221$ (200 fs) and $\sigma = 1240.23$ (30 fs). Unless otherwise noted, all the quantities in this paper are given in atomic units. In the following simulations, only resonant frequencies $\{\upsilon_l\}$ of the allowed transitions are included in the control fields, and the corresponding amplitudes $\{A_l\}$ and phases $\{\theta_l\}$ are optimized with a genetic algorithm [39]. The objective functional subjected to minimization is

$$J[E(t)] = |O[E(t),\eta] - O_T|^2 + \beta F \tag{21}$$

with

$$O[E(t),\eta] = \mathrm{Tr}[\rho(T_f)|b\rangle\langle b|] = \langle b|\rho(T_f)|b\rangle,$$
$$F = \sum_l (A_l)^2. \tag{22}$$

Here O_T is the target yield, and η is the coupling strength between the quantum system and the environment [see Eq. (4)]. By projecting the density matrix $\rho(T_f)$ at the final time T_f onto the target state $|b\rangle$, we can obtain the outcome $O[E(t),\eta]$ produced by the laser field $E(t)$ along with coupling to the environment of strength η. F is the fluence of the control field weighted by a positive constant β. Therefore, the minimization of the objective functional $J[E(t)]$ aims to achieve the target yield with a bias towards a lower laser intensity. In our previous work [36], cooperation between environmental processes and laser fields was found when seeking modest control yields O_T with a strongly interacting environment. The mechanistic origin of this finding was hidden in the overall dynamics, and HE-OD is employed here to reveal its nature.

A. Model (a)

The first model, (a), in Fig. 1 is a three-level system with target state $|3\rangle$, and the corresponding matrices in Eq. (4) are

$$H_0 = \begin{pmatrix} 0 & 0 & 0 \\ 0 & \omega_2 & 0 \\ 0 & 0 & \omega_3 \end{pmatrix}, \quad \mu = \begin{pmatrix} 0 & \mu_{12} & 0 \\ \mu_{12} & 0 & \mu_{23} \\ 0 & \mu_{23} & 0 \end{pmatrix},$$

$$L_1 = L_2^+ = \begin{pmatrix} 0 & \sqrt{\alpha_{12}} & 0 \\ 0 & 0 & 0 \\ 0 & 0 & 0 \end{pmatrix},$$

$$L_3 = L_4^+ = \begin{pmatrix} 0 & 0 & 0 \\ 0 & 0 & \sqrt{\alpha_{23}} \\ 0 & 0 & 0 \end{pmatrix},$$

where only Lindblad operators associated with the nearest-neighbor transitions are considered.

The matrix form in Liouville space of the Hamiltonian $\mathcal{H}(t)$ in Eq. (9) is

$$\mathcal{H}(t) = \begin{pmatrix} \beta_1 & \varepsilon_{12} & 0 & -\varepsilon_{12} & i\eta\alpha_{12} & 0 & 0 & 0 & 0 \\ \varepsilon_{12} & \beta_2 & \varepsilon_{23} & 0 & -\varepsilon_{12} & 0 & 0 & 0 & 0 \\ 0 & \varepsilon_{23} & \beta_3 & 0 & 0 & -\varepsilon_{12} & 0 & 0 & 0 \\ -\varepsilon_{12} & 0 & 0 & \beta_4 & \varepsilon_{12} & 0 & -\varepsilon_{23} & 0 & 0 \\ i\eta\alpha_{12} & -\varepsilon_{12} & 0 & \varepsilon_{12} & \beta_5 & \varepsilon_{23} & 0 & -\varepsilon_{23} & i\eta\alpha_{23} \\ 0 & 0 & -\varepsilon_{12} & 0 & \varepsilon_{23} & \beta_6 & 0 & 0 & -\varepsilon_{23} \\ 0 & 0 & 0 & -\varepsilon_{23} & 0 & 0 & \beta_7 & \varepsilon_{12} & 0 \\ 0 & 0 & 0 & 0 & -\varepsilon_{23} & 0 & \varepsilon_{12} & \beta_8 & \varepsilon_{23} \\ 0 & 0 & 0 & 0 & i\eta\alpha_{23} & -\varepsilon_{23} & 0 & \varepsilon_{23} & \beta_9 \end{pmatrix}, \tag{23}$$

with

$$\beta_1 = -i\eta\alpha_{12}, \quad \beta_2 = -\omega_2 - i\eta\left(\alpha_{12} + \frac{\alpha_{23}}{2}\right), \quad \beta_3 = -\omega_3 - \frac{i}{2}\eta(\alpha_{12} + \alpha_{23}), \quad \beta_4 = \omega_2 - i\eta\left(\alpha_{12} + \frac{\alpha_{23}}{2}\right),$$
$$\beta_5 = -i\eta(\alpha_{12} + \alpha_{23}), \quad \beta_6 = \omega_2 - \omega_3 - i\eta\left(\frac{\alpha_{12}}{2} + \alpha_{23}\right), \quad \beta_7 = \omega_3 - \frac{i}{2}\eta(\alpha_{12} + \alpha_{23}), \quad \beta_8 = \omega_3 - \omega_2 - i\eta\left(\frac{\alpha_{12}}{2} + \alpha_{23}\right),$$
$$\beta_9 = -i\eta\alpha_{23},$$

and $\varepsilon_{ij} = \mu_{ij}E(t)$. The parameters in the simulations are $\omega_2 = 0.036\,549\,3$, $\omega_3 = 0.065\,116\,4$, $\mu_{12} = 0.069\,061\,1$, $\mu_{23} = 0.083\,498\,5$, $\alpha_{12} = 0.0895$ and $\alpha_{23} = 0.1942$.

With the target yield O_T being 5% and the spectral amplitudes $\{A_l\}$ each having an upper limit 0.005, numerical simulations are performed to seek optimal laser fields for different decoherence strengths (η) and circumstances. As shown in Table I, there is clear evidence for cooperation between the dynamics induced by the laser field and the environment. For example, when $\eta = 4.8378 \times 10^{-8}$, the yield of the field optimized with the environment present [$O[E^{op}(t),\eta] = 5.00\%$] is much larger than that either through the environment acting alone ($O[E(t) = 0,\ \eta] = 2.07\%$) or in the case of the field alone ($O[E^{\mathrm{op}}(t),\ \eta = 0] = 0.92\%$), and the cooperative result of 5.00% is larger than the sum of the latter two yields (2.99%). The cooperation effect for modest control yields is consistent with a previous study [36], while the cooperative effect will generally be absent when seeking high yields, where the environment will often fight against the influence of the field. In the following, the case of $\eta = 4.8378 \times 10^{-8}$, giving the yield $O[E^{\mathrm{op}}(t) = 0,\ \eta] = 5\%$, is taken as the example to quantitatively identify the cooperation mechanism.

In order to illustrate the flexibility of HE-OD and its ability to give different perspectives on the mechanism, two types of encoding schemes are adopted for this open quantum system, and the encoding matrices are, respectively, taken to be

$$\Gamma_1 = \begin{pmatrix} 0 & 1 & 0 & 5 & 17 & 0 & 0 & 0 & 0 \\ 1 & 0 & 21 & 0 & 33 & 0 & 0 & 0 & 0 \\ 0 & 21 & 0 & 0 & 0 & 41 & 0 & 0 & 0 \\ 5 & 0 & 0 & 0 & 59 & 0 & 68 & 0 & 0 \\ 17 & 33 & 0 & 59 & 0 & 77 & 0 & 83 & 101 \\ 0 & 0 & 41 & 0 & 77 & 0 & 0 & 0 & 109 \\ 0 & 0 & 0 & 68 & 0 & 0 & 0 & 111 & 0 \\ 0 & 0 & 0 & 0 & 83 & 0 & 111 & 0 & 127 \\ 0 & 0 & 0 & 0 & 101 & 109 & 0 & 127 & 0 \end{pmatrix}$$

TABLE I. Yields (in percentage) of model (a) from various laser fields with different environmental strengths for the low objective yield of $O_T = 5.0\%$. The column "$O[E^{\rm op}(t),\eta]$" gives the yield from the optimal field $E^{\rm op}(t)$ determined in the presence of an environment of strength η; the column "$O[E(t)=0,\eta]$" is the yield obtained with the systemly driven by the environmental Lindblad term; the column "$O[E^{\rm op}(t),\eta=0]$" is the yield from the control field *alone*, where the field is determined in the presence of the Lindblad term at the specified value of η (i.e., the field is taken from the corresponding cases in the column labeled $O[E^{\rm op}(t),\eta]$). The yield with $E^{\rm op}(t)$ at $\eta = 0$ is only 2.68% due to the limitation on the field amplitudes in Eq. (20). The collective results show clear cooperation between the coherent dynamics and the environment, as explained in the text. The last column presents the fluence F determined from the optimal fields in the cases $O[E^{\rm op}(t),\eta]$, clearly showing that a diminished fluence is sufficient when the field cooperates with the environment.

η	$O[E^{\rm op}(t),\eta](\%)$	$O[E(t)=0,\eta](\%)$	$O[E^{\rm op}(t),\eta=0](\%)$	F
0.00	2.68	0.00	2.68	5.00×10^{-5}
1.20945×10^{-8}	5.02	0.61	2.55	4.875×10^{-5}
2.4189×10^{-8}	5.02	1.14	1.7	3.981×10^{-5}
4.8378×10^{-8}	5.00	2.07	0.92	2.850×10^{-5}

and

$$\Gamma_2 = \begin{pmatrix} 0 & 1 & 0 & 1 & 23 & 0 & 0 & 0 & 0 \\ 1 & 0 & 7 & 0 & 1 & 0 & 0 & 0 & 0 \\ 0 & 7 & 0 & 0 & 0 & 1 & 0 & 0 & 0 \\ 1 & 0 & 0 & 0 & 1 & 0 & 7 & 0 & 0 \\ 23 & 1 & 0 & 1 & 0 & 7 & 0 & 7 & 97 \\ 0 & 0 & 1 & 0 & 7 & 0 & 0 & 0 & 7 \\ 0 & 0 & 0 & 7 & 0 & 0 & 0 & 1 & 0 \\ 0 & 0 & 0 & 0 & 7 & 0 & 1 & 0 & 7 \\ 0 & 0 & 0 & 0 & 97 & 7 & 0 & 7 & 0 \end{pmatrix}.$$

The original Hamiltonian $\mathcal{H}(t)$ is non-Hermitian, as will be the case for its modulated form $\mathcal{H}(t,s)$. Despite the non-Hermitian nature of $\mathcal{H}(t)$ and $\mathcal{H}(t,s)$, both matrices are bounded such that the respective Dyson expansions converge in Eqs. (11) and (15). However, some numerical stability concerns can arise when solving the dynamical equations for $\mathcal{U}(t)$ and $\mathcal{U}(t,s)$. A similar special case of non-Hermetian modulation was treated in closed system dynamics [18]. The diagonal elements of Γ are all taken to be 0, corresponding to no modulation of the diagonal elements of $\mathcal{H}(t)$, and this was done to avoid numerical stability issues. These missing modulation terms correspond to "elastic" transitions of the type $\langle\langle ii|\mathcal{U}|ii\rangle\rangle$ in one or more places possibly occurring in the individual Dyson terms in Eq. (11). Although their presence will be hidden in the extracted pathway amplitudes, the lack of diagonal modulation will still permit determination of all key "inelastic" transitions (e.g., $\langle\langle ii|\mathcal{U}|jj\rangle\rangle$), including any relevant elastic contributions, in the mechanism. This conclusion is evident later from the fact that the extracted Dyson amplitudes sum up to the true value obtained by directly solving the Lindblad equation. In the first type of encoding scheme, Γ_1, each independent nonzero and nondiagonal element of the Hamiltonian $\mathcal{H}(t)$ (i.e., $\mathcal{H}_{ii',jj'}$) will be modulated by a specially chosen frequency (i.e., $\gamma_{ii',jj'}$). In particular, as mentioned in Sec. II, we select $\gamma_{ii',jj'}$ carefully so that each pathway of potential interest has a unique modulating frequency, $\gamma_{n(l'_{n-1}l_{n-1},l'_{n-2}l_{n-2},\ldots,l'_1l_1)}$, in Eq. (17). Table II shows the pathways extracted by HE-OD with amplitudes having magnitudes larger than 0.001. These significant pathway amplitudes all have essentially zero phase, thereby demonstrating a high degree of constructive interference regardless of the physical origin of the pathway leading to the target state. The pathways can be classified into three types: (i) dipole-induced pathways, (ii) dipole-environment-induced pathways, and (iii) exclusively environment-induced pathways. For example, the dipole-induced pathway $|11\rangle\rangle \to |12\rangle\rangle \to |13\rangle\rangle \to |23\rangle\rangle \to |33\rangle\rangle$ utilizes the two dipole operators (μ_{12} and μ_{23}) according to Eq. (23), the dipole-environment-induced pathway $|11\rangle\rangle \to |12\rangle\rangle \to |22\rangle\rangle \to |33\rangle\rangle$ exploits both the dipole operator μ_{12} and the Lindblad coupling term α_{23}, and the exclusively environment-induced pathway $|11\rangle\rangle \to |22\rangle\rangle \to |33\rangle\rangle$ is only related to the two Lindblad coupling terms α_{12} and α_{23}. We also note that symmetric pathways have the same magnitude

TABLE II. Magnitudes and phases of significant quantum pathway amplitudes of model (a) when $\eta = 4.8378\times10^{-8}$ in Table I with the encoding matrix Γ_1.

Type	Pathway	Pathway frequency	Magnitude	Phase
Dipole induced	$\|11\rangle\rangle \to \|12\rangle\rangle \to \|13\rangle\rangle \to \|23\rangle\rangle \to \|33\rangle\rangle$	172	1.222×10^{-3}	1.683×10^{-2}
	$\|11\rangle\rangle \to \|21\rangle\rangle \to \|31\rangle\rangle \to \|32\rangle\rangle \to \|33\rangle\rangle$	311	1.225×10^{-3}	-1.692×10^{-2}
	$\|11\rangle\rangle \to \|12\rangle\rangle \to \|22\rangle\rangle \to \|32\rangle\rangle \to \|33\rangle\rangle$	244	1.216×10^{-3}	6.861×10^{-2}
	$\|11\rangle\rangle \to \|21\rangle\rangle \to \|22\rangle\rangle \to \|23\rangle\rangle \to \|33\rangle\rangle$	250	1.221×10^{-3}	-6.776×10^{-2}
	$\|11\rangle\rangle \to \|12\rangle\rangle \to \|22\rangle\rangle \to \|23\rangle\rangle \to \|33\rangle\rangle$	220	1.195×10^{-3}	2.428×10^{-2}
	$\|11\rangle\rangle \to \|21\rangle\rangle \to \|22\rangle\rangle \to \|32\rangle\rangle \to \|33\rangle\rangle$	274	1.197×10^{-3}	-2.417×10^{-2}
Dipole environment induced	$\|11\rangle\rangle \to \|12\rangle\rangle \to \|22\rangle\rangle \to \|33\rangle\rangle$	135	9.069×10^{-3}	8.126×10^{-2}
	$\|11\rangle\rangle \to \|21\rangle\rangle \to \|22\rangle\rangle \to \|33\rangle\rangle$	165	9.069×10^{-3}	-8.126×10^{-2}
	$\|11\rangle\rangle \to \|22\rangle\rangle \to \|23\rangle\rangle \to \|33\rangle\rangle$	203	5.526×10^{-3}	-5.462×10^{-2}
	$\|11\rangle\rangle \to \|22\rangle\rangle \to \|32\rangle\rangle \to \|33\rangle\rangle$	227	5.525×10^{-3}	5.466×10^{-2}
Exclusively environment induced	$\|11\rangle\rangle \to \|22\rangle\rangle \to \|33\rangle\rangle$	118	2.045×10^{-2}	6.638×10^{-15}

TABLE III. Magnitudes and phases of significant quantum pathway amplitudes of model (a) with the encoding matrix Γ_2 for $\eta = 4.8378 \times 10^{-8}$ in Table I. The amplitude in each case reflects the sum of all terms of a particular pathway type; taking a sum of the amplitudes is meaningful, as the phases are all essentially 0. The results are in accord with summing the like pathway types in Table II.

Type	Pathway	Pathway frequency	Magnitude	Phase
Dipole induced	$\|11\rangle\rangle \to \|12\rangle\rangle \to \|13\rangle\rangle \to \|23\rangle\rangle \to \|33\rangle\rangle$	16	7.258×10^{-3}	-4.312×10^{-17}
	$\|11\rangle\rangle \to \|21\rangle\rangle \to \|31\rangle\rangle \to \|32\rangle\rangle \to \|33\rangle\rangle$			
	$\|11\rangle\rangle \to \|12\rangle\rangle \to \|22\rangle\rangle \to \|32\rangle\rangle \to \|33\rangle\rangle$			
	$\|11\rangle\rangle \to \|21\rangle\rangle \to \|22\rangle\rangle \to \|23\rangle\rangle \to \|33\rangle\rangle$			
	$\|11\rangle\rangle \to \|12\rangle\rangle \to \|22\rangle\rangle \to \|23\rangle\rangle \to \|33\rangle\rangle$			
	$\|11\rangle\rangle \to \|21\rangle\rangle \to \|22\rangle\rangle \to \|32\rangle\rangle \to \|33\rangle\rangle$			
Dipole environment induced	$\|11\rangle\rangle \to \|12\rangle\rangle \to \|22\rangle\rangle \to \|33\rangle\rangle$	99	1.808×10^{-2}	-2.033×10^{-14}
	$\|11\rangle\rangle \to \|21\rangle\rangle \to \|22\rangle\rangle \to \|33\rangle\rangle$			
	$\|11\rangle\rangle \to \|22\rangle\rangle \to \|23\rangle\rangle \to \|33\rangle\rangle$	37	1.103×10^{-2}	-2.537×10^{-15}
	$\|11\rangle\rangle \to \|22\rangle\rangle \to \|32\rangle\rangle \to \|33\rangle\rangle$			
Exclusively environment induced	$\|11\rangle\rangle \to \|22\rangle\rangle \to \|33\rangle\rangle$	120	2.045×10^{-2}	3.294×10^{-14}

and phases of opposite sign, although the latter difference is small. For example, pathways $|11\rangle\rangle \to |22\rangle\rangle \to |23\rangle\rangle \to |33\rangle\rangle$ and $|11\rangle\rangle \to |22\rangle\rangle \to |32\rangle\rangle \to |33\rangle\rangle$ only differ in the symmetric intermediate states $|23\rangle\rangle$ and $|32\rangle\rangle$. All of the amplitudes in Table II add up to give $\sim 5.68\%$, and the difference from the correct total value of $O[E^{\rm op}(t),\eta] = 5\%$ comes from a large set of other pathways (not shown here) with much lower amplitudes but with opposite phases $\sim \pi$. For example, the magnitudes for pathways $|11\rangle\rangle \to |22\rangle\rangle \to |12\rangle\rangle \to |22\rangle\rangle \to |33\rangle\rangle$ (pathway frequency, 184) and $|11\rangle\rangle \to |22\rangle\rangle \to |21\rangle\rangle \to |22\rangle\rangle \to |33\rangle\rangle$ (pathway frequency, 236) are both $\sim 0.6 \times 10^{-3}$, with respective phases $\sim \pi \pm 0.1 \times 10^{-1}$. Similarly, the respective magnitudes and phases of pathways$|11\rangle\rangle \to |22\rangle\rangle \to |23\rangle\rangle \to |22\rangle\rangle \to |33\rangle\rangle$ (pathway frequency, 272) and $|11\rangle\rangle \to |22\rangle\rangle \to |32\rangle\rangle \to |22\rangle\rangle \to |33\rangle\rangle$(pathway frequency, 284) are $\sim 0.75 \times 10^{-3}$ and $\sim \pi \pm 0.066 \times 10^{-1}$. The collective set of additional pathways makes a slightly destructive interference contribution, to finally yield the correct total amplitude of 5%. Thus, the dominant picture is one of constructive cooperative interactions between the dynamics induced by the field $E(t)$ and the environment.

With the first encoding scheme, Γ_1, symmetric transitions associated with the same dipole matrix element (i.e., $|11\rangle\rangle \to |12\rangle\rangle$ and $|11\rangle\rangle \to |21\rangle\rangle$ are both induced by μ_{12}) can be distinguished. However, this is not the case in the second type of encoding scheme, Γ_2, which produces a reduced image of the mechanism. The frequencies for μ_{12}, μ_{23}, α_{12}, and α_{23} are 1, 7, 23, and 97, respectively. Table III shows the extracted pathways and magnitudes of the amplitudes that are higher than 0.001. Their cooperative behavior can be clearly seen in their phases' all essentially being 0. The sum of the amplitudes of each separate class of pathways in Table II coincides with the corresponding summed values listed in Table III. This confirmation supports the freedom in choosing encoding schemes.

B. Model (b)

The second model (b) in Fig. 1 is a double-route open quantum system. We assume different decoherence strengths along the two routes, leading to the Lindblad equation's having the form

$$\frac{\partial \rho(t)}{\partial t} = -i[H_0 - \mu E(t), \rho(t)] + \eta_L \mathcal{F}_L\{\rho(t)\} + \eta_R \mathcal{F}_R\{\rho(t)\}, \tag{24}$$

with

$$\mathcal{F}_L\{\rho(t)\} = \sum_{j=1,\cdots,4} \left(L_j \rho L_j^+ - \frac{1}{2} L_j^+ L_j \rho - \frac{1}{2} \rho L_j^+ L_j \right) \tag{25}$$

and

$$\mathcal{F}_R\{\rho(t)\} = \sum_{j=5,\cdots,8} \left(L_j \rho L_j^+ - \frac{1}{2} L_j^+ L_j \rho - \frac{1}{2} \rho L_j^+ L_j \right). \tag{26}$$

The distinctions in Eqs. (25) and (26) reflect the prospect that different states can interact in particular ways with the environment, with accordingly distinct Lindblad operators and associated strengths η_L and η_R along the two routes [i.e., left and right, respectively, in Fig. 1(b)]. The target state is $|4\rangle$, and the corresponding model matrices in Eq. (24) are

$$H_0 = \begin{pmatrix} 0 & 0 & 0 & 0 \\ 0 & \omega_2 & 0 & 0 \\ 0 & 0 & \omega_3 & 0 \\ 0 & 0 & 0 & \omega_4 \end{pmatrix}, \quad \mu = \begin{pmatrix} 0 & \mu_{12} & \mu_{13} & 0 \\ \mu_{12} & 0 & 0 & \mu_{24} \\ \mu_{13} & 0 & 0 & \mu_{34} \\ 0 & \mu_{24} & \mu_{34} & 0 \end{pmatrix}, \quad L_1 = L_2^+ = \begin{pmatrix} 0 & \sqrt{\alpha_{12}} & 0 & 0 \\ 0 & 0 & 0 & 0 \\ 0 & 0 & 0 & 0 \\ 0 & 0 & 0 & 0 \end{pmatrix},$$

$$L_3 = L_4^+ = \begin{pmatrix} 0 & 0 & 0 & 0 \\ 0 & 0 & 0 & \sqrt{\alpha_{24}} \\ 0 & 0 & 0 & 0 \\ 0 & 0 & 0 & 0 \end{pmatrix}, \quad L_5 = L_6^+ = \begin{pmatrix} 0 & 0 & \sqrt{\alpha_{13}} & 0 \\ 0 & 0 & 0 & 0 \\ 0 & 0 & 0 & 0 \\ 0 & 0 & 0 & 0 \end{pmatrix}, \quad L_7 = L_8^+ = \begin{pmatrix} 0 & 0 & 0 & 0 \\ 0 & 0 & 0 & 0 \\ 0 & 0 & 0 & \sqrt{\alpha_{34}} \\ 0 & 0 & 0 & 0 \end{pmatrix},$$

where only Lindblad operators associated with the nearest-neighbor transitions are included.

The Hamiltonian $\mathcal{H}(t)$ in Liouville space is the 16×16 matrix

$$\mathcal{H}(t) = \begin{pmatrix}
\beta_1 & \varepsilon_{12} & \varepsilon_{13} & 0 & -\varepsilon_{12} & i\eta_L\alpha_{12} & 0 & 0 & -\varepsilon_{13} & 0 & i\eta_R\alpha_{13} & 0 & 0 & 0 & 0 & 0 \\
\varepsilon_{12} & \beta_2 & 0 & \varepsilon_{24} & 0 & -\varepsilon_{12} & 0 & 0 & 0 & -\varepsilon_{13} & 0 & 0 & 0 & 0 & 0 & 0 \\
\varepsilon_{13} & 0 & \beta_3 & \varepsilon_{34} & 0 & 0 & -\varepsilon_{12} & 0 & 0 & 0 & -\varepsilon_{13} & 0 & 0 & 0 & 0 & 0 \\
0 & \varepsilon_{24} & \varepsilon_{34} & \beta_4 & 0 & 0 & 0 & -\varepsilon_{12} & 0 & 0 & 0 & -\varepsilon_{13} & 0 & 0 & 0 & 0 \\
-\varepsilon_{12} & 0 & 0 & 0 & \beta_5 & \varepsilon_{12} & \varepsilon_{13} & 0 & 0 & 0 & 0 & 0 & -\varepsilon_{24} & 0 & 0 & 0 \\
i\eta_L\alpha_{12} & -\varepsilon_{12} & 0 & 0 & \varepsilon_{12} & \beta_6 & 0 & \varepsilon_{24} & 0 & 0 & 0 & 0 & 0 & -\varepsilon_{24} & 0 & i\eta_L\alpha_{24} \\
0 & 0 & -\varepsilon_{12} & 0 & \varepsilon_{13} & 0 & \beta_7 & \varepsilon_{34} & 0 & 0 & 0 & 0 & 0 & 0 & -\varepsilon_{24} & 0 \\
0 & 0 & 0 & -\varepsilon_{12} & 0 & \varepsilon_{24} & \varepsilon_{34} & \beta_8 & 0 & 0 & 0 & 0 & 0 & 0 & 0 & -\varepsilon_{24} \\
-\varepsilon_{13} & 0 & 0 & 0 & 0 & 0 & 0 & 0 & \beta_9 & \varepsilon_{12} & \varepsilon_{13} & 0 & -\varepsilon_{34} & 0 & 0 & 0 \\
0 & -\varepsilon_{13} & 0 & 0 & 0 & 0 & 0 & 0 & \varepsilon_{12} & \beta_{10} & 0 & \varepsilon_{24} & 0 & -\varepsilon_{34} & 0 & 0 \\
i\eta_R\alpha_{13} & 0 & -\varepsilon_{13} & 0 & 0 & 0 & 0 & 0 & \varepsilon_{13} & 0 & \beta_{11} & \varepsilon_{34} & 0 & 0 & -\varepsilon_{34} & i\eta_R\alpha_{34} \\
0 & 0 & 0 & -\varepsilon_{13} & 0 & 0 & 0 & 0 & 0 & \varepsilon_{24} & \varepsilon_{34} & \beta_{12} & 0 & 0 & 0 & -\varepsilon_{34} \\
0 & 0 & 0 & 0 & -\varepsilon_{24} & 0 & 0 & 0 & -\varepsilon_{34} & 0 & 0 & 0 & \beta_{13} & \varepsilon_{12} & \varepsilon_{13} & 0 \\
0 & 0 & 0 & 0 & 0 & -\varepsilon_{24} & 0 & 0 & 0 & -\varepsilon_{34} & 0 & 0 & \varepsilon_{12} & \beta_{14} & 0 & \varepsilon_{24} \\
0 & 0 & 0 & 0 & 0 & 0 & -\varepsilon_{24} & 0 & 0 & 0 & -\varepsilon_{34} & 0 & \varepsilon_{13} & 0 & \beta_{15} & \varepsilon_{34} \\
0 & 0 & 0 & 0 & 0 & i\eta_L\alpha_{24} & 0 & -\varepsilon_{24} & 0 & 0 & i\eta_R\alpha_{34} & -\varepsilon_{34} & 0 & \varepsilon_{24} & \varepsilon_{34} & \beta_{16}
\end{pmatrix},$$

with

$$\beta_1 = -i(\eta_L\alpha_{12} + \eta_R\alpha_{13}), \quad \beta_2 = -\omega_2 - i\left(\eta_L\alpha_{12} + \frac{\eta_R\alpha_{13} + \eta_L\alpha_{24}}{2}\right), \quad \beta_3 = -\omega_3 - i\left(\eta_R\alpha_{13} + \frac{\eta_L\alpha_{12} + \eta_R\alpha_{34}}{2}\right),$$

$$\beta_4 = -\omega_4 - \frac{i}{2}(\eta_L\alpha_{12} + \eta_R\alpha_{13} + \eta_L\alpha_{24} + \eta_R\alpha_{34}), \quad \beta_5 = \omega_2 - i\left(\eta_L\alpha_{12} + \frac{\eta_R\alpha_{13} + \eta_L\alpha_{24}}{2}\right), \quad \beta_6 = -i\eta_L(\alpha_{12} + \alpha_{24}),$$

$$\beta_7 = \omega_2 - \omega_3 - \frac{i}{2}(\eta_L\alpha_{12} + \eta_R\alpha_{13} + \eta_L\alpha_{24} + \eta_R\alpha_{34}), \quad \beta_8 = \omega_2 - \omega_4 - i\left(\eta_L\alpha_{24} + \frac{\eta_L\alpha_{12} + \eta_R\alpha_{34}}{2}\right),$$

$$\beta_9 = \omega_3 - i\left(\eta_R\alpha_{13} + \frac{\eta_L\alpha_{12} + \eta_R\alpha_{34}}{2}\right), \quad \beta_{10} = \omega_3 - \omega_2 - \frac{i}{2}(\eta_L\alpha_{12} + \eta_R\alpha_{13} + \eta_L\alpha_{24} + \eta_R\alpha_{34}), \quad \beta_{11} = -i\eta_R(\alpha_{13} + \alpha_{34}),$$

$$\beta_{12} = \omega_3 - \omega_4 - i\left(\eta_R\alpha_{34} + \frac{\eta_R\alpha_{13} + \eta_L\alpha_{24}}{2}\right), \quad \beta_{13} = \omega_4 - \frac{i}{2}(\eta_L\alpha_{12} + \eta_R\alpha_{13} + \eta_L\alpha_{24} + \eta_R\alpha_{34}),$$

$$\beta_{14} = \omega_4 - \omega_2 - i\left(\eta_L\alpha_{24} + \frac{\eta_L\alpha_{12} + \eta_R\alpha_{34}}{2}\right), \quad \beta_{15} = \omega_4 - \omega_3 - i\left(\eta_R\alpha_{34} + \frac{\eta_R\alpha_{13} + \eta_L\alpha_{24}}{2}\right), \quad \beta_{16} = -i(\eta_L\alpha_{24} + \eta_R\alpha_{34}),$$

and $\varepsilon_{ij} = \mu_{ij}E(t)$. The parameters of the system are $\omega_2 = 0.058\,396\,5$, $\omega_3 = 0.057\,313\,9$, $\omega_4 = 0.1171$, $\mu_{12} = 4.2275$, $\mu_{13} = 2.9931$, $\mu_{24} = 1.0216$, $\mu_{34} = 0.9$, $\alpha_{12} = 0.0895$, $\alpha_{24} = 0.1942$, $\alpha_{13} = 0.1164$, and $\alpha_{34} = 0.0885$.

In the optimizations, the target yield O_T and upper limit of the spectral amplitudes $\{A_l\}$ are, respectively, set to 5% and 0.00005. The results are listed in Table IV, and there is evidence for cooperation between the dynamics induced by the optimum field and the environment. For example, when $\eta_L = \eta_R = 2.4189 \times 10^{-8}$, the yield of the field determined in the presence of the environment is $O[E^{\rm op}(t), \eta_L, \eta_R] = 5.00\%$, which is much larger than for either the environment acting alone ($O[E(t) = 0, \eta_L, \eta_R] = 1.68\%$) or the field acting alone ($O[E^{\rm op}(t), \eta_L = \eta_R = 0] = 0.45\%$); the sum of the latter two cases (2.13%) is also much smaller than the situation producing 5.00% where the field and environment cooperate. The latter case of $O[E^{\rm op}(t), \eta_L, \eta_R] = 5.00\%$ at $\eta_L = \eta_R = 2.4189 \times 10^{-8}$ is subjected to an HE-OD mechanism analysis below.

TABLE IV. Yields (in percentage) of model (b) from various laser fields with different decoherence strengths for the low objective yield of $O_T = 5.0\%$. Due to the imposed constraints of pulse amplitudes $\{A_l\}$, the yield induced by the optimal field determined at $\eta_L = \eta_R = 0$ can only reach a value of 1.05%. The column "$O[E^{\rm op}(t),\eta_L,\eta_R]$" gives the yield from the optimal field $E^{\rm op}(t)$ determined in the presence of the environment of strengths η_L and η_R; the column "$O[E(t)=0,\eta_L,\eta_R]$" is the yield obtained with the system exclusively driven by the environmental Lindblad terms; the column "$O[E^{op}(t),\eta_L=\eta_R=0]$" is the yield from the control field without system-environmental coupling, but the control field is determined in the presence of the Lindblad term at specified values of η_L and η_R (i.e., the field comes from the corresponding cases in the column "$O[E^{\rm op}(t),\eta_L,\eta_R]$)." The collective results show clear cooperation between the coherent dynamics and the environment, as explained in the text. The last column gives the fluence F determined from the optimal fields in the cases $O[E^{\rm op}(t),\eta_L,\eta_R]$, showing that a modest reduction in fluence is still sufficient when the field cooperates with the environment.

η_L	η_R	$O[E^{\rm op}(t),\eta_L,\eta_R](\%)$	$O[E(t)=0,\eta_L,\eta_R](\%)$	$O[E^{\rm op}(t),\eta_L=\eta_R=0](\%)$	F
0.00	0.00	1.05	0.00	1.05	9.803×10^{-9}
2.4189×10^{-8}	0.00	5.00	1.14	0.662	8.911×10^{-9}
0.00	2.4189×10^{-8}	1.72	0.718	0.683	9.997×10^{-9}
2.4189×10^{-8}	2.4189×10^{-8}	5.00	1.68	0.45	9.153×10^{-9}

For simplicity of presentation, only the second type of encoding scheme described in Sec. III A is adopted here,

$$\Gamma_3 = \begin{pmatrix}
0 & 1 & 17 & 0 & 1 & 33 & 0 & 0 & 17 & 0 & 59 & 0 & 0 & 0 & 0 & 0 \\
1 & 0 & 0 & 3 & 0 & 1 & 0 & 0 & 0 & 17 & 0 & 0 & 0 & 0 & 0 & 0 \\
17 & 0 & 0 & 21 & 0 & 0 & 1 & 0 & 0 & 0 & 17 & 0 & 0 & 0 & 0 & 0 \\
0 & 3 & 21 & 0 & 0 & 0 & 0 & 1 & 0 & 0 & 0 & 17 & 0 & 0 & 0 & 0 \\
1 & 0 & 0 & 0 & 0 & 1 & 17 & 0 & 0 & 0 & 0 & 0 & 3 & 0 & 0 & 0 \\
33 & 1 & 0 & 0 & 1 & 0 & 0 & 3 & 0 & 0 & 0 & 0 & 0 & 3 & 0 & 42 \\
0 & 0 & 1 & 0 & 17 & 0 & 0 & 21 & 0 & 0 & 0 & 0 & 0 & 0 & 3 & 0 \\
0 & 0 & 0 & 1 & 0 & 3 & 21 & 0 & 0 & 0 & 0 & 0 & 0 & 0 & 0 & 3 \\
17 & 0 & 0 & 0 & 0 & 0 & 0 & 0 & 0 & 1 & 17 & 0 & 21 & 0 & 0 & 0 \\
0 & 17 & 0 & 0 & 0 & 0 & 0 & 0 & 1 & 0 & 0 & 3 & 0 & 21 & 0 & 0 \\
59 & 0 & 17 & 0 & 0 & 0 & 0 & 0 & 17 & 0 & 0 & 21 & 0 & 0 & 21 & 68 \\
0 & 0 & 0 & 17 & 0 & 0 & 0 & 0 & 0 & 3 & 21 & 0 & 0 & 0 & 0 & 21 \\
0 & 0 & 0 & 0 & 3 & 0 & 0 & 0 & 21 & 0 & 0 & 0 & 0 & 1 & 17 & 0 \\
0 & 0 & 0 & 0 & 0 & 3 & 0 & 0 & 0 & 21 & 0 & 0 & 1 & 0 & 0 & 3 \\
0 & 0 & 0 & 0 & 0 & 0 & 3 & 0 & 0 & 0 & 21 & 0 & 17 & 0 & 0 & 21 \\
0 & 0 & 0 & 0 & 0 & 42 & 0 & 3 & 0 & 0 & 68 & 21 & 0 & 3 & 21 & 0
\end{pmatrix},$$

where the modulating frequencies for μ_{12}, μ_{24}, μ_{13}, μ_{34}, α_{12}, α_{24}, α_{13}, and α_{34} are 1, 3, 17, 21, 33, 42, 59, and 68, respectively.

Table V lists the extracted pathway amplitudes whose magnitudes are larger than 0.001; only the amplitude sums are shown for each class of pathway. The dipole-environment-induced pathways have two types, with phases either near 0 or near π. There is overall constructive interference, with the pathway amplitudes having phases near 0 being dominant, although the amplitudes near π destructively interfere with the latter ones. As both types simply have phases of ~ 0 or $\sim \pi$, we may conclude clear balanced cooperation in the dynamical mechanism, regardless of its origin being in the system and/or the environment. We also note that the pathways modulated at frequencies 75 and 77, which are along the left route in Fig. 1(b), have the same net transition, $|11\rangle\rangle \rightarrow |22\rangle\rangle \rightarrow |44\rangle\rangle$, and thus can be assigned to the "composite pathway" $(|11\rangle\rangle \rightarrow |22\rangle\rangle \rightarrow |44\rangle\rangle)^*$, in accord with the analogous terminology in closed-system HE-OD analysis [18]. There are extra Rabi-like transitions along the pathways with frequency 77. For example, the mechanistic pathway $|11\rangle\rangle \rightarrow |12\rangle\rangle \rightarrow |11\rangle\rangle \rightarrow |22\rangle\rangle \rightarrow |44\rangle\rangle$ involves a transition from $|11\rangle\rangle$ to $|12\rangle\rangle$ and then a return from $|12\rangle\rangle$ back to $|11\rangle\rangle$. This Rabi flop is induced by the transition dipole operator μ_{12}. A related situation is along the right path in Fig. 1(b). The composite pathways of $(|11\rangle\rangle \rightarrow |33\rangle\rangle \rightarrow |44\rangle\rangle)^*$ have a lower amplitude than those of $(|11\rangle\rangle \rightarrow |22\rangle\rangle \rightarrow |44\rangle\rangle)^*$ (not shown in Table V). In summary, although mechanistic contributions along the left and right routes in Fig. 1(b) are not equal (i.e., due to distinctions in the dipole elements and Lindblad coefficients), they still cooperate to achieve the control goal. Similar behavior has been found in the optimal quantum control of a similar closed system [24].

IV. DISCUSSION AND CONCLUSIONS

The nature of control mechanisms in open system dynamics is of much interest in a variety of physical circumstances, and this paper extends the HE-OD methodology to allow for the treatment of such systems. The open-system HE-OD procedure illustrated here to analyze the population transfer in two simple multilevel systems may be easily generalized to more complex open systems, environments, observables, and, especially, non-Markovian models. In the present work, three types of pathways are studied: (i) dipole-induced pathways, (ii) dipole-dissipation-induced pathways, and (iii) exclusively

TABLE V. Magnitudes and phases of significant quantum pathways of model (b) with the encoding matrix Γ_3 when $\eta_L = \eta_R = 2.4189 \times 10^{-8}$. Only the sum of amplitudes is shown for each type of mechanism. Cooperation, including constructive and destructive interference, is evident, with the pathway phases being either ~ 0 or $\sim \pi$.

Type	Pathway	Pathway frequency	Magnitude	Phase
Dipole induced	$\|11\rangle\rangle \to \|12\rangle\rangle \to \|14\rangle\rangle \to \|24\rangle\rangle \to \|44\rangle\rangle$	8	2.279×10^{-3}	1.085×10^{-16}
	$\|11\rangle\rangle \to \|21\rangle\rangle \to \|41\rangle\rangle \to \|42\rangle\rangle \to \|44\rangle\rangle$			
	$\|11\rangle\rangle \to \|12\rangle\rangle \to \|22\rangle\rangle \to \|42\rangle\rangle \to \|44\rangle\rangle$			
	$\|11\rangle\rangle \to \|21\rangle\rangle \to \|22\rangle\rangle \to \|24\rangle\rangle \to \|44\rangle\rangle$			
	$\|11\rangle\rangle \to \|12\rangle\rangle \to \|22\rangle\rangle \to \|24\rangle\rangle \to \|44\rangle\rangle$			
	$\|11\rangle\rangle \to \|21\rangle\rangle \to \|22\rangle\rangle \to \|42\rangle\rangle \to \|44\rangle\rangle$			
Dipole environment induced	$\|11\rangle\rangle \to \|12\rangle\rangle \to \|22\rangle\rangle \to \|44\rangle\rangle$	44	3.443×10^{-2}	1.476×10^{-14}
	$\|11\rangle\rangle \to \|21\rangle\rangle \to \|22\rangle\rangle \to \|44\rangle\rangle$			
	$\|11\rangle\rangle \to \|12\rangle\rangle \to \|11\rangle\rangle \to \|12\rangle\rangle \to \|22\rangle\rangle \to \|44\rangle\rangle$	46	5.009×10^{-3}	$\pi + 4.441 \times 10^{-15}$
	$\|11\rangle\rangle \to \|12\rangle\rangle \to \|11\rangle\rangle \to \|21\rangle\rangle \to \|22\rangle\rangle \to \|44\rangle\rangle$			
	$\|11\rangle\rangle \to \|12\rangle\rangle \to \|22\rangle\rangle \to \|12\rangle\rangle \to \|22\rangle\rangle \to \|44\rangle\rangle$			
	$\|11\rangle\rangle \to \|12\rangle\rangle \to \|22\rangle\rangle \to \|21\rangle\rangle \to \|22\rangle\rangle \to \|44\rangle\rangle$			
	$\|11\rangle\rangle \to \|21\rangle\rangle \to \|22\rangle\rangle \to \|12\rangle\rangle \to \|22\rangle\rangle \to \|44\rangle\rangle$			
	$\|11\rangle\rangle \to \|21\rangle\rangle \to \|22\rangle\rangle \to \|21\rangle\rangle \to \|22\rangle\rangle \to \|44\rangle\rangle$			
	$\|11\rangle\rangle \to \|21\rangle\rangle \to \|11\rangle\rangle \to \|12\rangle\rangle \to \|22\rangle\rangle \to \|44\rangle\rangle$			
	$\|11\rangle\rangle \to \|21\rangle\rangle \to \|11\rangle\rangle \to \|21\rangle\rangle \to \|22\rangle\rangle \to \|44\rangle\rangle$			
	$\|11\rangle\rangle \to \|12\rangle\rangle \to \|11\rangle\rangle \to \|22\rangle\rangle \to \|44\rangle\rangle$	77	2.641×10^{-3}	$\pi - 2.857 \times 10^{-14}$
	$\|11\rangle\rangle \to \|21\rangle\rangle \to \|11\rangle\rangle \to \|22\rangle\rangle \to \|44\rangle\rangle$			
	$\|11\rangle\rangle \to \|22\rangle\rangle \to \|21\rangle\rangle \to \|22\rangle\rangle \to \|44\rangle\rangle$			
	$\|11\rangle\rangle \to \|22\rangle\rangle \to \|12\rangle\rangle \to \|22\rangle\rangle \to \|44\rangle\rangle$			
	$\|11\rangle\rangle \to \|13\rangle\rangle \to \|11\rangle\rangle \to \|12\rangle\rangle \to \|22\rangle\rangle \to \|44\rangle\rangle$	78	1.848×10^{-3}	$\pi + 5.136 \times 10^{-15}$
	$\|11\rangle\rangle \to \|31\rangle\rangle \to \|11\rangle\rangle \to \|12\rangle\rangle \to \|22\rangle\rangle \to \|44\rangle\rangle$			
	$\|11\rangle\rangle \to \|13\rangle\rangle \to \|11\rangle\rangle \to \|21\rangle\rangle \to \|22\rangle\rangle \to \|44\rangle\rangle$			
	$\|11\rangle\rangle \to \|31\rangle\rangle \to \|11\rangle\rangle \to \|21\rangle\rangle \to \|22\rangle\rangle \to \|44\rangle\rangle$			
	$\|11\rangle\rangle \to \|13\rangle\rangle \to \|33\rangle\rangle \to \|44\rangle\rangle$	102	4.670×10^{-3}	1.778×10^{-14}
	$\|11\rangle\rangle \to \|31\rangle\rangle \to \|33\rangle\rangle \to \|44\rangle\rangle$			
Exclusively environment induced	$\|11\rangle\rangle \to \|22\rangle\rangle \to \|44\rangle\rangle$	75	1.031×10^{-2}	3.945×10^{-15}
	$\|11\rangle\rangle \to \|33\rangle\rangle \to \|44\rangle\rangle$	127	6.336×10^{-3}	-7.565×10^{-15}

dissipation-induced pathways. Under the conditions studied with a strongly interacting environment, the extracted pathway amplitudes show that the three types of pathways generally interfere constructively when modest control yields are sought. The detailed cooperation between the optimal laser fields and the environment identified by HE-OD is consistent with the previous conclusion [36], although the origin of the phenomenon was not understood before. Naturally, upon the seeking of high yields cooperation will likely break down, but HE-OD may be applied as well in these circumstances to reveal the detailed nature of the mechanism. In our work, only Lindblad operators associated with nearest-neighbor transitions are considered. Moreover, the dephasing effect associated with diagonal Lindblad operators is absent in the present model. For simulations of non-Markovian quantum systems, master equations involving memory terms appear, and even more complex models may be necessary in some cases. Nevertheless, the general HE-OD principles and procedures may be appropriately extended to analyze the mechanistic pathway dynamics for any such models.

HE-OD for open systems could be amenable to experimental implementation with appropriate operations. Experimental demonstration of HE-OD in closed systems has already been realized by modulating the field, and the same procedure would apply to the system (i.e., Hamiltonian) portion of the dynamical mechanism analysis of open dynamics. For a fuller picture of the mechanism, access to environmental modulation will also need to be available. In many situations, the sample temperature or pressure can be readily manipulated as a partial form of environmental modulation. In this circumstance, the environmental modulation consists in dialing the overall strength of the environmental interactions by modulating η in Eq. (4) (e.g., in the context of a gas phase system colliding with the atoms or molecules of a buffer gas, an increase in pressure results in a corresponding increase in the collision rate). It is also possible to perform a series of experiments in which the types of atoms or molecules that make up the environment are systematically changed (i.e., similarly to changing the "solvent" containing the system under study). This situation may allow addressing some specific matrix elements of the Lindblad operator (e.g., by systematically choosing environmental atoms or molecules with increasing environmental medium polarizability that could strengthen the coupling to the system's electronic states). It is similar to the modulation introduced in this paper, but with only a discrete number of points (i.e., there is no continuous way of modulating the environment in this fashion). On the other hand, in some situations it may be feasible to dynamically modulate the environment (e.g., through separate encoded field excitation that has a negligible direct effect on the system) in much the same fashion as done with the control interacting with the system itself. In this case there may be continuous access

over some of the matrix elements of the Lindblad operator, allowing for environmental modulation similar to that outlined in this paper.

In conclusion, we have introduced a practical tool for the study of environmental interactions and demonstrated its application in the context of numerical simulations of the Lindblad equation. The versatility of HE-OD can enable a variety of additional analyses of open-system dynamics simulations as well as the prospect of direct implementation in the laboratory.

ACKNOWLEDGMENTS

This work was supported by the National Natural Science Foundation of China (Grants No. 61203061, No. 61403362, No. 61374091, and No. 61473199). H.R. acknowledges the support from the Chinese Academy of Sciences President's International Fellowship Initiative (No. 2015VTA008) and additional support from the U.S. Department of Energy (Grant No. DE-FG02-02ER15344). R.R. acknowledges support from the U.S. Army Research Office (Grant No. W911NF-13-1-0237).

[1] H. Rabitz, R. de Vivie-Riedle, M. Motzkus, and K. Kompa, Science **288**, 824 (2000).
[2] J. L. Herek, W. Wohlleben, R. J. Cogdell, D. Zeidler, and M. Motzkus, Nature **417**, 533 (2002).
[3] Y. Silberberg, Annu. Rev. Phys. Chem. **60**, 277 (2009).
[4] J. Zhang, Y. X. Liu, R. B. Wu, C. W. Li, and T. J. Tarn, Phys. Rev. A **82**, 022101 (2010).
[5] J. Zhang, Y. X. Liu, and F. Nori, Phys. Rev. A **79**, 052102 (2009).
[6] H. M. Wiseman and A. C. Doherty, Phys. Rev. Lett. **94**, 070405 (2005).
[7] H. Mabuchi, Phys. Rev. A **78**, 032323 (2008).
[8] G. G. Gillett, R. B. Dalton, B. P. Lanyon, M. P. Almeida, M. Barbieri, G. J. Pryde, J. L. O' Brien, K. J. Resch, S. D. Bartlett, and A. G. White, Phys. Rev. Lett. **104**, 080503 (2010).
[9] C. Altafini and F. Ticozzi, IEEE Trans. Auto. Cont. **57**, 1898 (2012).
[10] C. Brif, M. D. Grace, M. Sarovar, and K. C. Young, New J. Phys. **16**, 065013 (2014).
[11] S. J. Glaser, U. Boscain, T. Calarco, C. P. Koch, Walter Köckenberger, R. Kosloff, I. Kuprov, B. Luy, S. Schirmer, T. Schulte-Herbrüggen, D. Sugny, and F. K. Wilhelm, Eur. Phys. J. D **69**, 279 (2015).
[12] J. Petersen, R. Mitrić, V. Bonačić-Koutecký, J.P. Wolf, J. Roslund, and H. Rabitz, Phys. Rev. Lett. **105**, 073003 (2010).
[13] T. Brixner, N. H. Damrauer, P. Niklaus, and G. Gerber, Nature **414**, 57 (2001).
[14] R. J. Gordon and S. A. Rice, Annu. Rev. Phys. Chem. **48**, 601 (1997).
[15] D. G. Kuroda, C. P. Singh, Z. Peng, and V. D. Kleiman, Science **326**, 263 (2009).
[16] K. Hoki and P. Brumer, Phys. Rev. Lett. **95**, 168305 (2005).
[17] P. van der Walle, M. T. W. Milder, L. Kuipers, and J. L. Herek, Proc. Natl. Acad. Sci. USA **106**, 7714 (2009).
[18] A. Mitra and H. Rabitz, Phys. Rev. A **67**, 033407 (2003).
[19] A. Mitra, I. R. Solá, and H. Rabitz, Phys. Rev. A **67**, 043409 (2003).
[20] A. Mitra and H. Rabitz, J. Chem. Phys. **125**, 194107 (2006).
[21] A. Mitra and H. Rabitz, J. Chem. Phys. **128**, 044112 (2008).
[22] A. Mitra, I. R. Solá, and H. Rabitz, Phys. Rev. A **77**, 043415 (2008).
[23] R. Rey-de-Castro and H. Rabitz, Phys. Rev. A **81**, 063422 (2010).
[24] F. Gao, R. Rey-de-Castro, A. M. Donovan, J. Xu, Y. Wang, H. Rabitz, and F. Shuang, Phys. Rev. A **89**, 023416 (2014).
[25] R. Rey-de-Castro, R. Cabrera, D. I. Bonder, and H. Rabitz, New J. Phys. **15**, 025032 (2013).
[26] R. Rey-de-Castro, Z. Leghtas, and H. Rabitz, Phys. Rev. Lett. **110**, 223601 (2013).
[27] F. Gao, Y. Wang, R. Rey-de-Castro, H. Rabitz, and F. Shuang, Phys. Rev. A **92**, 033423 (2015).
[28] B. H. Liu, L. Li, Y. F. Huang, C. F. Li, G. C. Guo, E. M. Laine, H. P. Breuer, and J. Piilo, Nat. Phys. **7**, 931 (2011).
[29] K. Khodjasteh, D. A. Lidar, and L. Viola, Phys. Rev. Lett. **104**, 090501 (2010).
[30] J. Zhang, R. B. Wu, Y. X. Liu, C. W. Li, and T. J. Tarn, IEEE Trans. Auto. Cont. **57**, 1997 (2012).
[31] R. Schmidt, A. Negretti, J. Ankerhold, T. Calarco, and J. T. Stockburger, Phys. Rev. Lett. **107**, 130404 (2011).
[32] J. Zhang, Y. X. Liu, R. B. Wu, K. Jacobs, and F. Nori, Phys. Rev. A **87**, 032117 (2013).
[33] W. Cui, Z. R. Xi, and Y. Pan, Phys. Rev. A **77**, 032117 (2008).
[34] C. Altafini, Phys. Rev. A **70**, 062321 (2004).
[35] J. Zhang, R. B. Wu, C. W. Li, and T. J. Tarn, IEEE Trans. Auto. Cont. **55**, 619 (2010).
[36] F. Shuang and H. Rabitz, J. Chem. Phys. **124**, 154105 (2006).
[37] G. Lindblad, Commun. Math. Phys. **48**, 119 (1976).
[38] S. Mukamel, *Principles of Nonlinear Optical Spectroscopy Oxford University* (Oxford University Press, New York, 1995).
[39] D. E. Goldberg, *Genetic Algorithms in Search, Optimization, and Machine Learning* (Addison–Wesley, Reading, MA, 1989).